A particle-in-cell plus Monte Carlo study of plasma-induced damage of normal incidence collector optics used in extreme ultraviolet lithography

R. C. Wieggers, W. J. Goedheer,[a] M. R. Akdim, and F. Bijkerk
FOM-Institute for Plasma Physics Rijnhuizen, P.O. Box 1207, 3430 BE, Nieuwegein, The Netherlands

P. A. Zegeling
Faculty of Science, Utrecht University, P.O. Box 80010, 3508 TA Utrecht, The Netherlands

(Received 28 July 2007; accepted 6 November 2007; published online 14 January 2008)

We present a kinetic simulation of the plasma formed by photoionization in the intense flux of an extreme ultraviolet lithography (EUVL) light source. The model is based on the particle-in-cell plus Monte Carlo approach. The photoelectric effect and ionization by electron collisions are included. The time evolution of the low density argon plasma is simulated during and after the EUV pulse and the ion-induced sputtering of the coating material of a normal incidence collector mirror is computed. The relation between the time and position at which the ions are created and their final energy is studied, revealing how the evolution and the properties of the sheath influence the amount of sputtered material. The influence of the gas pressure and the source intensity is studied, evaluating the behavior of Ar^+ and Ar^{2+} ions. A way to reduce the damage to the collector mirror is presented. © *2008 American Institute of Physics*. [DOI: 10.1063/1.2829783]

I. INTRODUCTION

In semiconductor industries there is a continuous demand for printing smaller structures on silicon wafers. To accomplish this, the wavelength of the radiation used for imaging is reduced down to the extreme ultraviolet (EUV), namely, to 13.5 nm. Although the use of these shorter wavelengths is one of the most promising methods to fulfill the demands, it faces a number of technological challenges.

In EUV lithograpy (EUVL) tools[1] a powerful pulsed EUV light source is used, typically operating at a frequency of 2.5–10 kHz and a pulse duration of 100 ns. The collector, being the first optical element in the system, is a critical component. To meet commercial demands, a collector lifetime of 3000 h for so-called consumable to 15000 h for nonconsumable mirrors is needed.[2] The collector is exposed to by far the highest photon flux. Apart from heating, this flux promotes oxidation and formation of carbonaceous impurities by photochemical processes. Another problem is the debris emitted by the source.[3] To capture the debris, solutions like a foil trap are being developed,[4] and also a heavy buffer gas like argon is needed. Photoionization of this buffer gas leads to plasma generation, and, possibly, to damage of the collector surface by ion-induced sputtering.

Although these EUVL tools are operated at low background gas pressures, the absorption of a small fraction of the EUV radiation will still result in the generation of a low density plasma (10^{15}–10^{17} m^{-3}) that contains energetic electrons. A part of the relatively more mobile electrons will be lost at the walls, resulting in a positive space charge in front of the optical elements. In this region of positive space charge, ions are accelerated toward the collector, and may obtain an energy in excess of the threshold for sputtering of the surface material. A protective layer of ruthenium is frequently applied to reduce the damage, although other candidates for this so-called capping layer exist.[5,6]

In this paper, we present a study of plasma-induced sputtering damage to the collector, using a spherical 3d3v particle-in-cell (PIC) Monte Carlo model. A kinetic model is needed because of the low plasma density, lack of equilibrium, complex energy distributions, and strong time dependence. Extending previous work[6–8] for a planar geometry, we study the behavior of the ions in more detail and switch to a spherical geometry, relevant for a normal incidence collector. Being the first reflective optics after the source, this collector will be exposed to the most extreme conditions in EUVL tools. The conclusions of this paper address at what particular time during the pulse, and at what particular distance from the collector, the ions are created that cause most of the damage. A scan in pressure and source intensity shows the influence of these parameters on the plasma evolution and the energy obtained by the ions. Finally, a way to increase the lifetime of the collector is presented.

II. MODEL DESCRIPTION

A. Particle-in-cell model

The basic idea behind a PIC model[9] is to follow test particles (ions and electrons) in time. Each particle represents a large number of real particles (its weight). The charge density, potential, and electric field are represented on a computational grid, enabling a self-consistent calculation of the forces on the charged particles. The weight of a test particle is adjusted during the simulation to keep the statistical fluctuations in the charge density and in the number of collisions within acceptable limits.

Figure 1 shows one complete step of the PIC Monte Carlo model. Using the leapfrog scheme,[9] at every time step the position and velocity of each test particle are updated. The behavior of each test particle is governed by the classical

[a]Electronic mail: goedheer@rijnhuizen.nl.

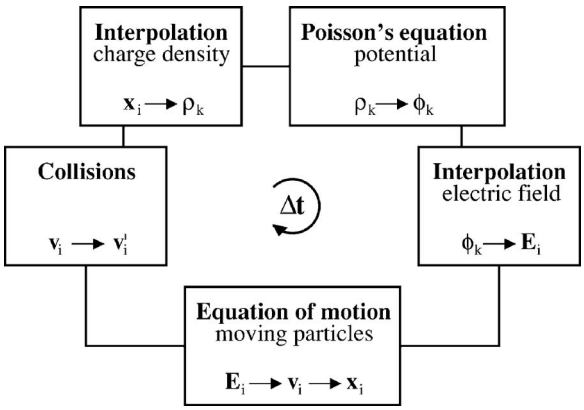

FIG. 1. PIC Monte Carlo scheme. The charge density (ρ) needed to calculate the electric field (E) is obtained by interpolation of the charge of each particle onto a computational grid. The electric field is interpolated back to the position of the particles (x), in order to update their velocity (v). After performing Monte Carlo collisions, this scheme is repeated every time step Δt.

laws of physics, where the magnetic field is neglected. The charge of each particle is linearly interpolated onto a computational grid, yielding the net charge density required to determine the potential and the electric field. The electric field is again linearly interpolated to the position of each particle.

Since the source can be seen as a point source, a one dimensional spherical geometry is used, see Fig. 2. The area between two concentric spheres with radii 3 and 8 cm is simulated. This corresponds to the area between the debris filter (foil trap) and the collector. We have chosen this rather limited size to facilitate comparison with previous calculations in a planar geometry[6,7] and to keep the computational effort within reasonable limits. As discussed in Sec. III, we found similar results when we take a larger distance and a higher source intensity. Note that the use of a point source results in a gradient in plasma density in the radial direction. The electric field is calculated in one dimension; the positions and velocities of the particles are traced in the three dimensional Cartesian system. In this geometry, cells correspond to the volume between two concentric spheres with radii r and $r+\Delta r$. To calculate the potential and electric field

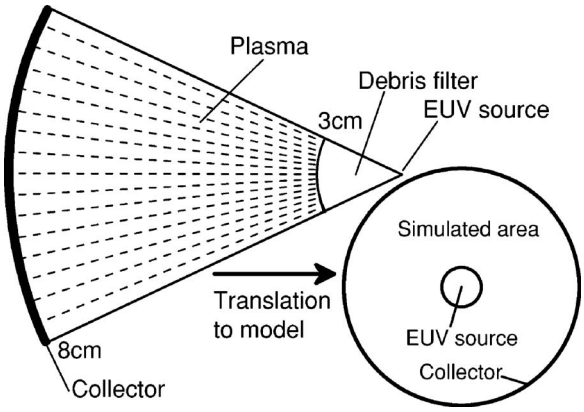

FIG. 2. On the left, a typical EUV setup of a source and normal incidence collector is shown. This is modeled by simulating the plasma between two concentric spheres, as shown on the right.

the one dimensional Poisson equation in spherical coordinates is solved and the radial electric field is calculated according to

$$\frac{\partial^2 \phi}{\partial r^2} = \frac{1}{r^2}\frac{\partial}{\partial r}\left(r^2 \frac{\partial \phi}{\partial r}\right) = -\frac{\rho}{\epsilon_0}, \quad E = -\frac{\partial \phi}{\partial r}, \tag{1}$$

where ϵ_0 is the permittivity in vacuum and $\rho = e(\Sigma_i Z_i n_i - n_e)$ is the net charge density. Both boundaries of the plasma, the debris filter and the collector, are assumed to be grounded.

B. Plasma generation

Plasma is produced by photoionization of the background gas (yielding ions and electrons) and by the photoelectric effect at the collector surface (yielding electrons). The electrons thus generated can obtain enough energy (either directly at creation or after acceleration by the electric field) to ionize the gas by collisions. The photoionization rate almost linearly depends on both the background gas pressure and source intensity, while the electron influx from the photoelectric effect only depends on the source intensity. The number of photoionization events in a shell between two points of our computational grid is constant, so the generated plasma density decreases with distance from the debris filter.

1. Photoionization

The EUV photon energy (92 eV) exceeds the threshold for single, double, and triple photoionizations of argon given by $E_s = 15.8$ eV, $E_d = 43.4$ eV, and $E_t = 84.3$ eV, respectively. According to Refs. 10 and 11 the probability of triple ionization is more than two orders of magnitude less than single ionization, so it is neglected here. The total cross section for 92 eV photons, $\sigma_{\text{tot}} = 1.37 \times 10^{-22}$ m^2, is divided over single and double ionizations according to $\sigma_s = 1.16 \times 10^{-22}$ m^2 and $\sigma_d = 2.1 \times 10^{-23}$ m^2.[12]

To conserve momentum, most of the photon energy will be transferred to the electrons. The ion energy therefore equals the energy of the neutral argon atom, and is sampled from a Maxwellian distribution at room temperature ($T = 300$ K). The energy available for the electrons is the photon energy minus the threshold energy. In the case of single photoionization, the electron energy is $h\nu - E_s = 76.2$ eV, while for double ionization $h\nu - E_d = 48.6$ eV is randomly divided over the two electrons. The velocity of the charged particles at creation is assumed to have an isotropic distribution.

Only a very small fraction (typically $<1\%$) of the photons is absorbed by the background gas. Therefore, we take the background density constant in space and time and the probability of absorption independent of the distance to the source. The number of photoionization events per pulse (N_{pi}) is given by

$$N_{\text{pi}} = \frac{I}{h\nu}\{1 - \exp[-n_{\text{bg}}\sigma_{\text{tot}} L(1 + R_{ml})]\}, \tag{2}$$

where I is the radiated energy in joules per pulse, n_{bg} the background density, L the distance between the debris filter and the collector, and $R_{ml} = 0.68$ the reflection coefficient of the collector.

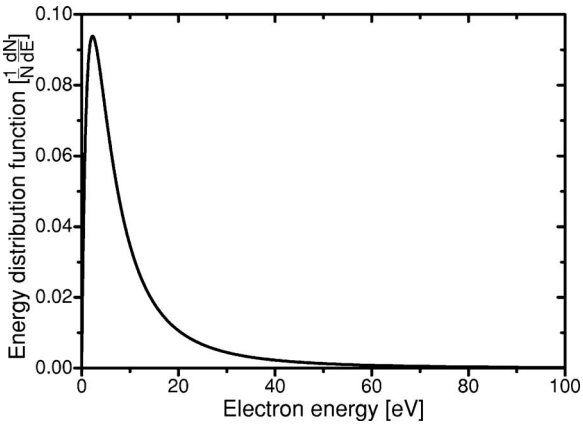

FIG. 3. Secondary electron energy distribution at emission from ruthenium. The secondary electron energy does not depend on the photon energy and is typically a few eV (Ref. 13).

A source will in practice be far from monochromatic, as we assumed here. Substantial emission may occur at wavelengths longer than 13.5 nm and a part of this emission is easily absorbed and will enhance the photoionization. What will happen in detail depends on the emission spectrum of the source. This is shortly discussed in Sec. III, where we present our conclusions.

2. Photoelectric effect

Photons, absorbed by the collector, will free a primary electron below the surface, with an energy of $h\nu - W = 85.26$ eV, where W (6.74 eV) is the work function of ruthenium. Such an energetic primary electron will release one or more secondary electrons by electron-electron collisions in the solid. After many collisions, in which most of the kinetic energy is lost, a secondary electron can be emitted from the collector surface into the plasma. The energy of an emitted electron E_e again depends on the work function. Figure 3 shows the energy distribution of the emitted electrons for ruthenium given by[13]

$$S(E_e, W) = \frac{W^2 E_e}{(E_e + W)^4}. \tag{3}$$

The most likely electron energy equals $W/3$. Only 2.1% of the 92 eV photons incident on ruthenium results in the emission of a secondary electron from the surface. The probability of absorption directly at the surface, followed by emission of a primary electron with the full energy, is negligibly small.[14] The direction of the velocity vector of the emitted electrons is sampled isotropically away from the collector.

C. Monte Carlo collisions

The Monte Carlo collision method is based on random numbers and simulates collisions by adjusting the velocity of test particles in both magnitude and direction. Every time step a fraction of all test particles will be selected to collide. This fraction is the ratio between the time step of the simulation and the average time between collisions. For every colliding particle, the collision type is randomly selected according to its relative contribution to the total cross section. For inelastic collisions the magnitude of the velocity is adapted according to the loss of kinetic energy. Then the scattering angle is sampled randomly, in agreement with the differential cross section of the selected collision type. The scattering angle has an isotropic distribution for ion impact collisions. For electron impact collisions the distribution depends on the energy and becomes increasingly anisotropic for high energies.[15] It is sampled according to

$$\theta = \arccos\left(1 - \frac{2R}{1 + 8\varepsilon(1-R)}\right), \tag{4}$$

where $R \in U(0,1)$ and $\varepsilon = E/27.21$ is the normalized energy.

Since the plasma density is low compared to the neutral density, collisions between charged particles and three-body collisions can be neglected. The only relevant collisions are those between charged particles and the neutral background gas. The following processes are taken into account:

$$e^- + \mathrm{Ar} \rightarrow 2e^- + \mathrm{Ar}^+ (\text{ionization}, -15.8\ \text{eV})$$

$$e^- + \mathrm{Ar} \rightarrow e^- + \mathrm{Ar}(\text{elastic})$$

$$e^- + \mathrm{Ar} \rightarrow e^- + \mathrm{Ar}^* (\text{excitation}, -11.5\ \text{eV})$$

$$\mathrm{Ar}^+ + \mathrm{Ar} \rightarrow \mathrm{Ar} + \mathrm{Ar}^+ (\text{charge exchange})$$

$$\mathrm{Ar}^{i+} + \mathrm{Ar} \rightarrow \mathrm{Ar}^{i+} + \mathrm{Ar}(\text{elastic}, i = 1,2)$$

The total electron collision frequency[16] is more than an order of magnitude higher than the total ion collision frequency. For energetic electrons ionization is the dominant collision process. It cools the electrons rapidly. In spite of the low ion collision frequency, charge exchange could be important, since it can slow down an accelerated ion just before impinging upon the collector. For simplicity, the elastic ion collision frequency of multiply charged ions is taken equal to that of Ar^+. Probably this collision frequency is underestimated, but by lack of references, this is a much more realistic option than assuming no multiply charged ion collisions at all.

D. Timescales and plasma behavior

At the start of the 100 ns pulse, there is no plasma between the debris filter and the collector. During the pulse a small fraction of the photons will be absorbed by the background gas, resulting in the creation of ions and electrons in this region. An additional electron flux from the collector surface is created by the photoelectric effect. This results in a negative space charge in the first few millimeters in front of the collector. Here ions are accelerated inward, and electrons outward, toward the collector. On this timescale no damage by sputtering ions is expected.

Just after the pulse, when plasma production by photon absorption has stopped, the negative space charge disappears. Because of the much higher mobility of the electrons, a region with net positive space charge develops in front of the collector (the plasma sheath). The electric field in this sheath strongly accelerates the ions toward the collector. The

TABLE I. Model parameters: The values of the background density and source intensity are the reference values. For the scans also twice and four times these values are used. The source intensity I_0 corresponds to a radiated energy I of 2.44×10^{-2} J per pulse and a repetition frequency of 10 kHz.

Background density	n_{bg}	1.2×10^{20} m^{-3}
Corresponding pressure	p_0	0.5 Pa
Average source intensity	I_0	244 W (in 4π sr)
Photon energy	$h\nu$	92 eV
Pulse duration	τ	100 ns
Pulse frequency	f	10 kHz
Simulated time		1000 ns

potential difference between the collector and the bulk plasma, the sheath potential, is directly related to the average electron energy in the bulk plasma.

Passing the same potential difference, doubly charged ions will have picked up twice as much energy as singly charged ions when they arrive at the collector. Because of their higher kinetic energy, the doubly charged ions will be present in this narrow sheath region for a shorter period of time.

Since ions are very slow, only ions produced in the sheath region will possibly damage the collector. Ions from further away arrive when the sheath has collapsed again and do not gain enough energy. Therefore, we briefly discuss the behavior of this sheath. The thickness of a plasma sheath is linearly correlated to the Debye length $\lambda_D \sim \sqrt{\bar{E}/n_e}$, with $\bar{E}$ the mean electron energy. This implies that the sheath thickness, and with it the region where ions are produced that might damage the collector, decreases with increasing plasma density. Both an increase of the source intensity and of the pressure enhance the density and should have this effect. A higher pressure in addition enhances the collision frequency of particles in the plasma. Therefore, electrons will be cooled faster by inelastic collisions. A lower average electron energy leads to a narrower sheath and a lower sheath potential. This reduces both the amount of fast ions and their impact energy.

III. RESULTS AND DISCUSSION

Two parameter scans are done to study the effects discussed above. Starting from a reference pressure p_0 and source intensity I_0, the source intensity is increased by factors of 2 and 4, keeping the pressure at p_0, and the pressure is increased by the same factors, keeping the source intensity at I_0. Table I shows the reference parameters. The source intensity is expressed here as the average power radiated into 4π sr. With a repetition frequency of 10 kHz, the radiated power I is 2.44×10^{-2} J per pulse. During the 100 ns pulse the intensity at the collector surface is 3 MW m^{-2}. The value of I_0 is chosen such that the plasma density in the spherical geometry of our model is similar to the density in the planar geometry used in Refs. 6 and 7 At the collector optics, this choice of I_0 corresponds within one order of magnitude to the intensity required by industry at the intermediate focus.[17]

First, we present some results of the simulation with the reference parameters given in Table I. Figure 4(a) shows the potential at different times. During the pulse, at $t<100$ ns, the potential is negative in a small region in front of the collector. From $t>100$ ns, the potential first increases, and then decreases. The increase is due to the fact that just after the pulse many of the electrons, produced by the photoelectric effect, will leave the plasma, leaving a region of positive net charge behind. After this, the potential starts to decrease, because the electrons lose their energy in inelastic collisions.

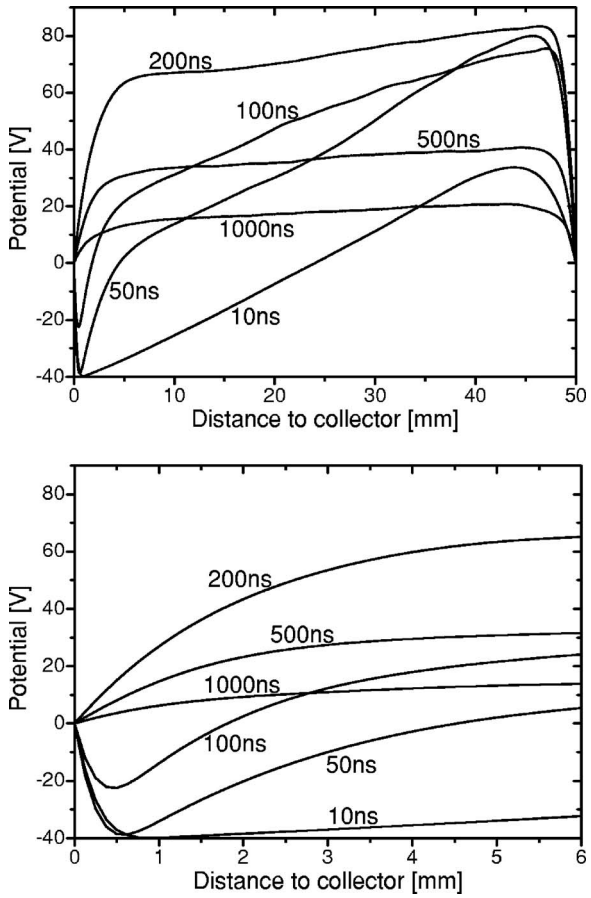

FIG. 4. Full potential profiles (a, upper) and profiles close to the collector (b,lower). During the pulse, at $t<100$ ns, the potential is negative in front of the collector. From $t>100$ ns, the potential first increases, because electrons are lost at the collector. After this, the potential decreases since the electrons lose their energy in inelastic collisions.

Figure 4(b) shows a close-up of the potential just in front of the collector. Ions are accelerated toward lower potentials. During the pulse the ions will be trapped in the potential dip in front of the collector, and only during a few hundred nanoseconds after the pulse the ions are likely to impinge upon the collector with a relatively high energy. Note the short distance of only a few millimeters in which ions are strongly accelerated toward the collector.

Figure 5 shows how the Ar^+ and Ar^{2+} impact energy depends on the time since the start of the pulse and the distance from the collector at which they are created. The maximum impact energy is just above 37 eV for Ar^+ and is 88 eV for Ar^{2+}. The energy of the ions is more than twice that of Ar^+ ions because they have a higher velocity and therefore spend less time in the sheath. Since the sheath potential decreases in time after the pulse, the Ar^{2+} ions move through a larger time-averaged potential difference. The faster motion of the Ar^{2+} ions is also responsible for the shift in the posi-

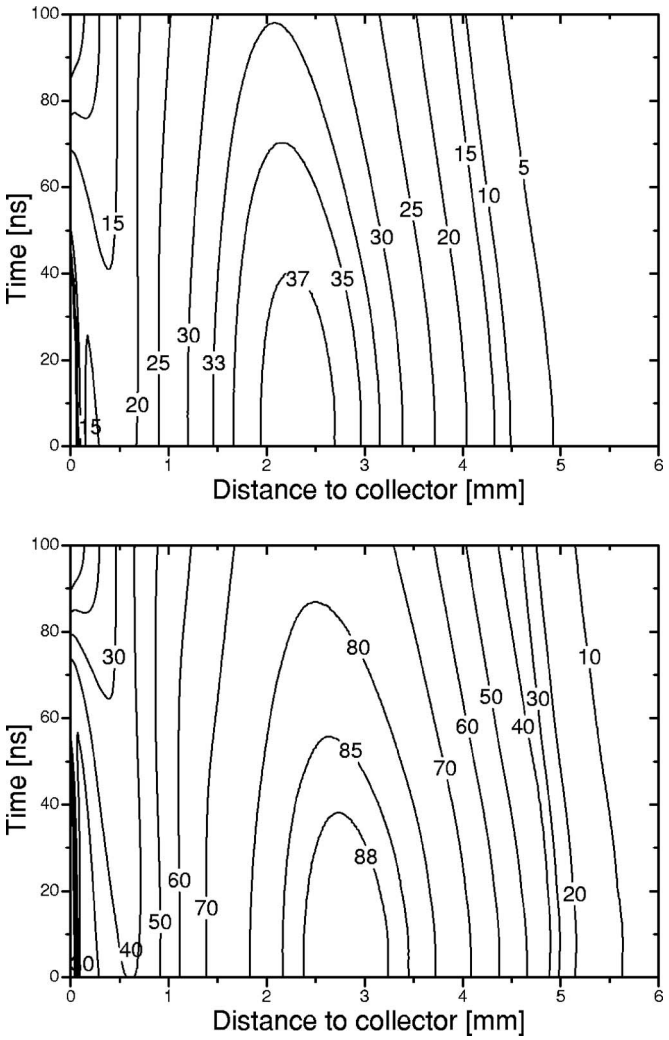

FIG. 5. Impact energy of Ar^+ (a, upper) and Ar^{2+} (b, lower) ions as a function of the time and position at which they are created.

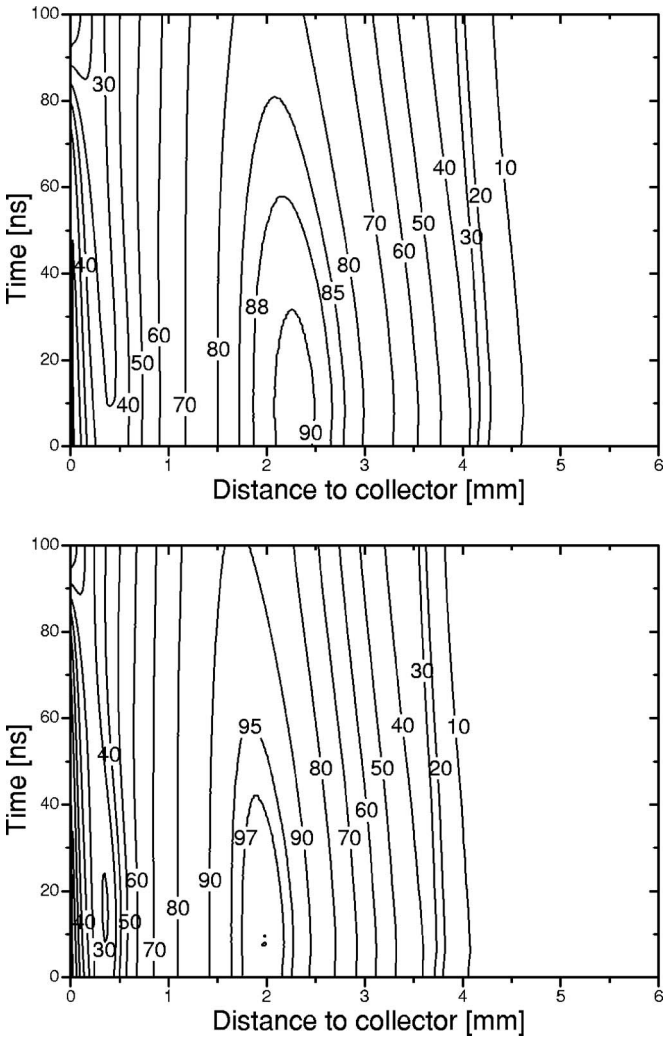

FIG. 6. Ar^{2+} impact energy as function of the time and position at the moment of creation for two (a, upper) and four (b, lower) times the reference intensity. At higher source intensities the maximum impact energy increases, while the size of the critical area in which ions are strongly accelerated decreases.

tion of the maximum in Fig. 5. This is at around 3 mm from the collector for Ar^{2+} and between 2 and 2.5 mm for Ar^+ and merely reflects the longer distance Ar^{2+} ions travel during the buildup and decay of the sheath. An important result of our modeling is that the ions that obtain the highest impact energies are produced at the start of the pulse. Ions produced very close to the collector, that is, between the collector and potential dip, are first accelerated toward this dip. Reversal of their velocity toward the collector takes so long that they are never accelerated to high energies.

Figure 6 shows similar results with intensities factors of 2 and 4 higher. Here only the results for Ar^{2+} are discussed, since this type of ions is the most damaging. Note that the higher the source intensity, the closer to the collector the ions are produced that obtain the maximum impact energy. This effect is caused by the higher plasma density, leading to lower values of λ_D and a narrower sheath.

Another important observation is the increasing maximum impact energy for increasing source intensity. This can again be explained by the decreased sheath thickness, resulting in a shorter transit time, and a higher time-averaged sheath potential.

Next, we will increase the pressure, keeping the source intensity at the reference value. Again only the behavior of the doubly charged ions will be discussed. The influence of a pressure increase on the plasma density is similar to an increase of the source intensity. The important difference is that, due to the higher pressure, the collision frequency of the charged particles in the plasma increases, leading to a faster decrease of the kinetic energy of the electrons. The plasma temperature, that is, the mean electron energy, decreases faster, and with that the sheath potential. Therefore, the ions feel a relatively low potential difference before impinging upon the collector, resulting in lower ion impact energies. Another beneficial effect of the lower electron temperature is the shorter Debye length. This reduces the sheath thickness and the critical area in which ions are strongly accelerated toward the collector.

Figure 7 shows the Ar^{2+} impact energy for higher pressures. The influence on the maximum impact energy and the size of the critical area is clearly visible.

For all cases studied in this paper, the damage to the collector is shown in Fig. 8. The number of pulses needed to

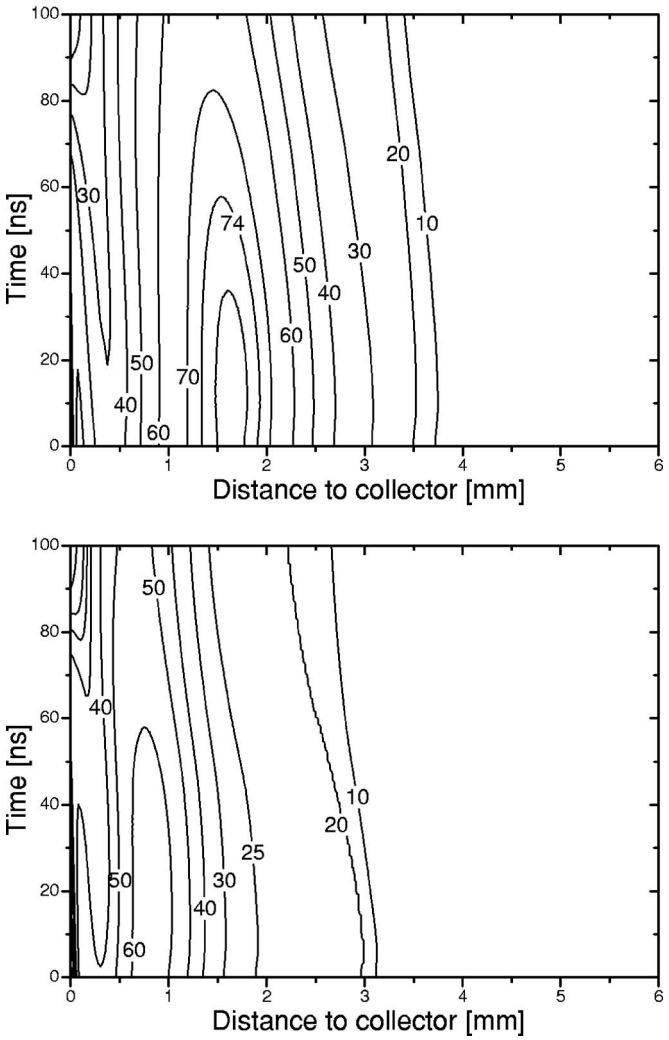

FIG. 7. Ar^{2+} impact energy as function of the time and position at the moment of creation for two (a, upper) and four (b, lower) times the reference pressure. A higher pressure leads to faster cooling of the electrons. This reduces the sheath thickness and the sheath potential. The maximum impact energy decreases and the critical area in which ions are strongly accelerated decreases even more than at an increase of the source intensity.

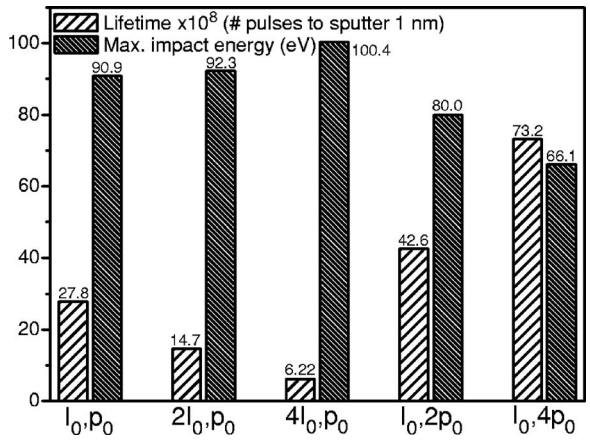

FIG. 8. The maximum impact energy and the lifetime of the collector expressed in number of pulses to remove 1 nm of the protective layer for the different simulations. Small variations in the maximum impact energy result in much higher variations in lifetime.

sputter 1 nm of the protective layer is determined. To calculate the damage to the collector by a single pulse, the sputtering yield given by Yamamura and Tawara[18] has been used. This sputtering yield of argon ions on ruthenium has a threshold around 27 eV and increases strongly beyond this threshold. Ions impacting with an energy above 50 eV damage the collector by several orders of magnitude more than ions with energies near threshold. As Fig. 8 shows, it is very important to reduce the ion energy. Even a reduction by only a few eV results in a strong reduction in damage by sputtering and a significant increase in collector lifetime.

The behavior as simulated for a relatively small distance between the EUV source and the collector will not change drastically when this distance is enlarged. An increase of the radius R_c of the outer sphere in the simulations will lead to more plasma formation by photoionization, but the volume of the shells increases as well. In fact, the amount of plasma generated in a shell with a given thickness remains the same, so the plasma density will decrease near the collector. If the intensity of the source is increased proportional to R_c^2, roughly the same plasma density and sheath properties are to be expected in front of the optics, because also the amount of secondary electrons generated per m^2 is the same. The geometry approaches that of a planar mirror, as simulated previously.[6,7] Simulations for a mirror radius of 12 cm instead of 8 cm showed that the intensity should be enhanced more than $\propto R^2$ to obtain the same sputtering damage per m^2 of the collector. The flatter geometry reduces the electric fields, extending the region with a negative potential during the pulse. The physics issues discussed for the smaller system remain, however, especially the supralinear increase of the damage with increasing intensity and the beneficial effects of a higher pressure. A full parameter scan is beyond the scope of this paper and will be addressed in the near future.

The influence of photons with a larger wavelength strongly depends on the spectrum of the source. Unclassified data are scarce and thus again a scan would be required, with a spectrum characterized with a number of parameters. Some predictions can be made, however, by considering the results of the simulations presented here. Photons with a lower energy will be absorbed more easily,[12] leading to a higher plasma density and narrower sheaths. The electrons generated have less kinetic energy, so the sheath potential and the sheath width will decrease. This is similar to what happens when the pressure is increased. Both effects are beneficial when considering the damage to the collector. However, if the sheath becomes much narrower, the ion transit time decreases and the ions feel a larger time-averaged potential difference, giving higher impact energies. Also the increase in the ion flux toward the collector will lead to more damage. Probably, the negative effects are more than compensated for by the reduction of the maximum impact energy.

IV. CONCLUSIONS

PIC Monte Carlo modeling was successfully used to investigate the sputtering capabilities of an argon plasma generated by energetic photons in an EUVL tool. The influence of the source intensity and the pressure on the acceleration of ions in the sheath region and the resulting sputtering of the

collector optics was studied. Increasing the source intensity results in a supralinear growth of the damage by ion-induced sputtering, while increasing the pressure leads to a significant decrease in the damage and an extension of the collector lifetime. This is correlated with a similar behavior of the maximum impact energy of the plasma ions.

The results can be understood from the evolution of the space charge sheath in front of the collector, during and just after the EUV photon pulse. Through the Debye length, the sheath width is determined by the plasma density and the average electron energy.

Due to higher plasma densities, established by an increase of either the source intensity or the background pressure, the sheath thickness is reduced. Therefore at a higher plasma density, the region where ions are created that damage the collector will be reduced and ions will pass the sheath in a shorter period of time. In this shorter period the potential decreases less, and thus the ion impact energy increases. For a higher pressure, the faster cooling of the electrons has two effects. The sheath thickness is reduced even more and the potential decreases faster. This potential decrease leads to a lower ion impact energy and reduction of the damage.

The impact energy of doubly charged ions is more than twice the impact energy of singly charged ions due to the shorter transit time through the sheath. Ar^{2+} ions, especially those produced at the start of the pulse, are responsible for by far most of the sputtering damage, while Ar^{+} ions barely exceed the sputtering threshold. Faster cooling of the plasma, in this paper realized by increasing the pressure, is crucial to reduce or even prevent sputtering of optical elements like the collector. This opens a way to enhance their lifetime significantly.

ACKNOWLEDGMENTS

This work is part of the FOM Industrial Partnership Programme I10 ("XMO") which is carried out under contract with Carl Zeiss SMT AG, Oberkochen and the "Stichting voor Fundamenteel Onderzoek der Materie (FOM)," the latter being financially supported by the "Nederlandse Organisatie voor Wetenschappelijk Onderzoek (NWO)" and SenterNovem through the "ACHieVE" and EAGLE programmes coordinated by ASML.

[1] H. Meiling, H. Meijer, V. Banine, R. Moors, and R. Groeneveld, Proc. SPIE **6151**, 615108 (2006).
[2] V. Banine and H. Voorma, *Requirements and Prospects of Next Generation Extreme Ultraviolet Sources for Lithography Applications*, Oral Presentation at the 2006 International EUVL Symposium, Barcelona, Spain, 15–18 October 2006, available at www.sematech.org.
[3] C. de Bruin, Ph.D. thesis, Eindhoven University of Technology, 2004.
[4] L. Shmaenok, C. de Bruijn, H. Fledderus, R. Stuik, A. Schmidt, D. Simanovskii, A. Sorokin, T. Andreeva, and F. Bijkerk, Proc. SPIE **3331**, 90 (1998).
[5] T. Madey, N. Faradzhev, B. Yakshinskiy, and N. Edwards, Appl. Surf. Sci. **253**, 1691 (2006).
[6] M. H. L. van der Velden, W. J. M. Brok, J. J. A. M. van der Mullen, W. J. Goedheer, and V. Banine, Phys. Rev. E **73**, 036406 (2006).
[7] M. H. L. van der Velden, W. J. M. Brok, J. J. A. M. van der Mullen, and V. Banine, J. Appl. Phys. **100**, 073303 (2006).
[8] R. C. Wieggers, W. J. Goedheer, E. Louis, and F. Bijkerk, Proc. SPIE **6586**, 65860L (2007).
[9] C. Birdsall and A. Langdon, *Plasma Physics via Computer Simulation* (Hilger, London, 1991).
[10] N. Saito and I. H. Suzuki, Int. J. Mass Spectrom. Ion Process. **115**, 157 (1992).
[11] J. B. Bluett, D. Lukić, and R. Wehlitz, Phys. Rev. A **69**, 042717 (2004).
[12] B. Henke, E. Gullikson, and J. Davis, At. Data Nucl. Data Tables **54**, 181 (1993).
[13] B. Henke, J. Smith, and D. Attwood, J. Appl. Phys. **48**, 1852 (1977).
[14] B. V. Yakshinskiy, R. Wasielewski, E. Loginova, and T. E. Madey, Proc. SPIE **6517**, 65172Z (2007).
[15] A. Okhrimovskyy, A. Bogaerts, and R. Gijbels, Phys. Rev. E **65**, 037402 (2002).
[16] A. Phelps and Z. Petrovic, Plasma Sources Sci. Technol. **8**, R21 (1999).
[17] N. Harned, M. Goethals, R. Groeneveld, P. Kuerz, M. Lowisch, H. Meijer, H. Meiling, K. Ronse, J. Ryan, M. Tittnich, H. Voorma, and J. D. Zimmerman, Proc. SPIE **6517**, 651706 (2007).
[18] Y. Yamamura and H. Tawara, At. Data Nucl. Data Tables **62**, 149 (1996).